

Ring-Opening Polymerization

Highly Stereocontrolled Ring-Opening Polymerization of Racemic Alkyl β -Malolactonates Mediated by Yttrium [Amino-alkoxy-bis(phenolate)] ComplexesCédric G. Jaffredo, Yulia Chapurina, Evgueni Kirillov, Jean-François Carpentier,* and Sophie M. Guillaume*^[a]

Abstract: Yttrium [amino-alkoxy-bis(phenolate)]amido complexes have been used for the ring-opening polymerization (ROP) of racemic alkyl β -malolactonates (4-alkoxycarbonyl-2-oxetanones, *rac*-MLA^Rs) bearing an allyl (All), benzyl (Bz) or methyl (Me) lateral ester function. The nature of the *ortho*-substituent on the phenolate rings in the metal ancillary dictated the stereocontrol of the ROP, and consequently the syndiotactic enrichment of the resulting polyesters. ROP promoted by catalysts with halogen (Cl, Br)-disubstituted ligands allowed the first reported synthesis of highly syndiotactic PMLA^Rs ($P_r \geq 0.95$); conversely, catalysts bearing bulky alkyl and aryl *ortho*-substituted ligands proved largely inef-

fective. All polymers have been characterized by ¹H and ¹³C{¹H} NMR spectroscopy, MALDI-ToF mass spectrometry and DSC analyses. Statistical and thermal analyses enabled the rationalization of the chain-end control mechanism. Whereas the stereocontrol of the polymerization obeyed a Markov first-order (Mk1) model for the ROP of *rac*-MLA^{Bz} and *rac*-MLA^{All}, the ROP of *rac*-MLA^{Me} led to a chain end-control of Markov second-order type (Mk2). DFT computations suggest that the high stereocontrol ability featured by catalysts bearing Cl- and Br-substituted ligands does not likely originate from halogen bonding between the halogen substituent and the growing polyester chain.

Introduction

Control of monomer sequence in polymers is of fundamental importance. Hence, Nature is able to encode information directly within the internal structure of macromolecules, as in proteins or DNA. Strategies to control monomer sequences and to adapt encoding techniques to synthetic polymers are of topical interest.^[1] One possibility is based on the use of mixed batches of monomers. In particular, highly controlled sequence polymers can be obtained from the stereocontrolled ring-opening polymerization (ROP) of 50:50 mixtures of two different chiral monomers of opposite absolute configuration. As initially developed by Coates, Thomas, and co-workers with nonfunctional β -lactones (β -butyrolactone and higher alkyl or fluoroalkyl derivatives)^[2] and further enlarged by our group to

alkyl β -malolactonates (4-alkoxycarbonyl-2-oxetanones),^[3] this strategy afforded highly alternating poly(β -hydroxyalkanoate) (PHA)-based copolymers (> 95% alternation). Extension of the concept to mixtures of functional β -lactones enabled the synthesis and post-polymerization modification of copolymers with alternating *chemically differentiated* monomer units; the fragmentation by MS/MS ESI evidenced the alternating unzipping of both repeating units in these original PHA chains.^[3] This effective synthetic strategy relies on the use of highly syndioselective ROP yttrium catalysts, which are able to focus on the asymmetric center “regardless” of the nature of the lateral function of the monomer; the approach is so far limited to chemically closely related monomers. With the aim to extend the range of applications of this attractive approach, the development of highly syndioselective catalysts that are applicable to a broad array of monomers, along with an understanding of the sequence control mechanism, both appear mandatory.^[4,5]

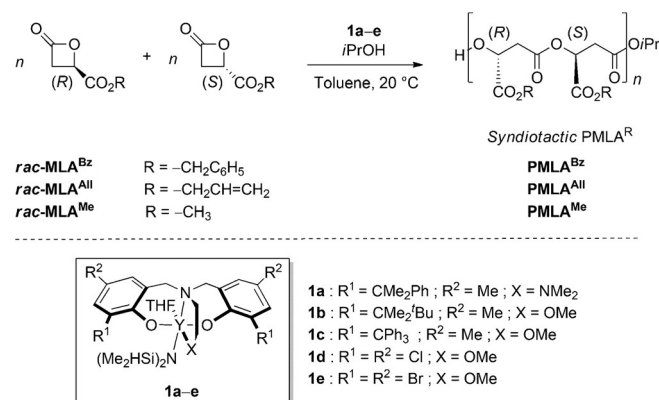
To this end, we and others have developed complexes based on oxophilic metals that are highly active and syndioselective catalysts for the ROP of lactones.^[6–9] The class of [amino-alkoxy-bis(phenolate)]yttrium-amido complexes, in the presence of an alcohol (typically isopropanol) as co-initiator, has shown remarkable stereoselectivities for the ROP of racemic lactide (*rac*-LA) and racemic β -butyrolactone (*rac*-BL), thereby affording highly enriched heterotactic poly(lactic acid) (PLA) and syndiotactic poly(3-hydroxybutyrate) (PHB) (P_r , probability of racemic linkage > 0.95), respectively.^[10] Tuning of the steric and electronic features of the phenolate *ortho*-substitu-

[a] Dr. C. G. Jaffredo, Dr. Y. Chapurina, Dr. E. Kirillov, Prof. Dr. J.-F. Carpentier, Dr. S. M. Guillaume
Institut des Sciences Chimiques de Rennes
Organometallics: Materials and Catalysis Laboratories
UMR 6226 CNRS-Université de Rennes 1
Campus de Beaulieu, 35042 Rennes Cedex (France)
E-mail: jean-francois.carpentier@univ-rennes1.fr
sophie.guillaume@univ-rennes1.fr

Supporting information and ORCID from the author for this article are available on the WWW under <http://dx.doi.org/10.1002/chem.201600223>. It contains supporting synthetic procedures, ¹H, ¹³C{¹H} and DOSY NMR data, MALDI-ToF mass spectra, DSC analyses, and statistical analysis of stereosequences in PMLA^Rs synthesized from complexes **1**, and computational details including Cartesian coordinates of computed structures.

ents in these ligands modulates the metal environment and consequently the extent of stereocontrol of the sequence of the repeating units, and ultimately the physicochemical behavior of the recovered polymers. Although bulkiest substituents basically led to the highest degree of heterotacticity in the ROP of *rac*-LA, experimental observations coupled with computational investigations pinpointed the role of both steric and electronic parameters to reach the highest syndioselectivity in the ROP of *rac*-BL.^[8d,10]

In this paper, we report on the use of a series of [amino-alkoxy-bis(phenolate)]yttrium-amido complexes in combination with *i*PrOH for the syndioselective ROP of several β -malolactonates, namely racemic benzyl β -malolactonate (*rac*-MLA^{Bz}), racemic allyl β -malolactonate (*rac*-MLA^{All}), and racemic methyl β -malolactonate (*rac*-MLA^{Me}; Scheme 1), complementing our pre-



Scheme 1. Syndioselective ROP of *rac*-MLA^Rs mediated by **1a–e**/*i*PrOH systems (complex **1e** was generated in situ from proligand **5** and Y(N(SiHMe₂)₃(THF) and not isolated).

liminary results on this chemistry.^[3] This manuscript provides comprehensive and detailed results on catalyst comparison, polymer microanalysis, and mechanism analysis. The catalyst systems promoted the efficient synthesis of the corresponding PMLA^Rs, with—quite uniquely in this chemistry—the complexes with halogen-disubstituted ligands affording the highest syndiotacticities ($P_r > 0.95$). Some DFT computations aimed at exploring the relationship between the nature of the substituent on the catalyst and its syndioselectivity are also reported.

Results and Discussion

Stereoselective ROP of *rac*-MLA^{Bz}, *rac*-MLA^{All}, and *rac*-MLA^{Me}

The performance of five [amino-alkoxy-bis(phenolate)]yttrium-amido complexes (**1a–e**; complex **1e** was generated in situ from proligand **5** and Y(N(SiHMe₂)₃(THF) and not isolated; previous work in this series has established that strictly equivalent polymerization performances are obtained upon using either isolated or in situ generated complexes^[3,8d]) featuring sterically and electronically differentiated ancillaries was investigated in the ROP of several racemic alkyl β -malolactonates

(*rac*-MLA^Rs, R = Bz, All, Me; Scheme 1). The most significant data for the thus prepared homopolymers are gathered in Table 1, Table 2, and Table 3.

ROP of *rac*-MLA^{Bz} was first investigated at a [monomer]₀/[catalyst]₀ ratio of 100 in the presence of 1 equiv of *i*PrOH co-initiator at 20 °C in toluene. All yttrium complexes **1a–e** showed good activity, with complex **1a** being the most active (full conversion within 2 min; that is, TOF ≥ 3000 h⁻¹; Table 1, entry 3). To our knowledge, this catalytic system is the most active described to date for the ROP of *rac*-MLA^{Bz}.^[11] The catalyst system based on **1b** offered an activity one order of magnitude lower (TOF = 360 h⁻¹, Table 1, entry 7), yet slightly better than that of systems based on complexes **1c–e** under the same conditions (TOF = 40–50 h⁻¹, Table 1, entries 9, 12 and 15, respectively). These reactivity differences likely reflect the major influence of the fourth group in the metal ancillary; that is, NMe₂ in **1a** versus OMe in **1b–e**. A quite good agreement between the theoretical molar mass values ($M_{n,theo}$) and the experimental values determined by NMR ($M_{n,NMR}$) was observed with all catalytic systems. The molar mass values determined by SEC ($M_{n,SEC}$) using polystyrene standards were always approximately double the $M_{n,NMR}$ values, thus suggesting a correction factor of ca. 0.5 to account for the difference in hydrodynamic volume between PMLA^{Bz} and polystyrene. The dispersities remained generally narrow ($D_M = 1.06–1.54$), indicating a relatively fast and quantitative initiation along with limited undesirable side reactions (intermolecular (reshuffling), intramolecular (back-biting) transesterification reactions, or other transfer reactions). Nevertheless, the dispersities were found to be quite dependent on the catalytic system, with the alkyl-substituted catalysts leading to lower dispersity values ($D_{M,1a-c} = 1.06–1.29$) as compared with the halogen-substituted catalysts ($D_{M,1d-e} = 1.44–1.54$). Hence, the catalyst system based on **1a** afforded the best activity as well as the best control over the molar mass values. In the absence of alcohol co-initiator, the amido complexes showed comparable performances to those observed in the presence of 1 equiv *i*PrOH (Table 1, entries 5, 8, 10, and 13). The good control over the polymerization reaction by using **1a**/*i*PrOH was further evidenced by the linear variation of $M_{n,NMR}$ values with the amount of monomer consumed for a [*rac*-MLA^{Bz}]₀/[**1a**]₀ ratio in the range of 25–100 (Table 1, entries 1–3; Figure 1). This linear increase is in fair agreement with the $M_{n,theo}$ values calculated assuming one growing chain for each catalyst/co-initiator couple, thus highlighting some living character of the polymerization. On the other hand, when the monomer loading was increased to [*rac*-MLA^{Bz}]₀/[**1a**]₀ = 500, no polymer was formed (Table 1, entry 4); this most likely highlighted the high sensitivity of these yttrium catalysts to residual impurities present in such a large batch of polar monomer.^[12] Experiments carried out in THF rather than in toluene failed to lead to any monomer conversion (Table 1, entry 6 vs. entry 5, respectively). This result can be rationalized by competitive coordination of THF versus monomer onto the metallic center. Such behavior has previously been reported in the ROP of alike polar cyclic ester monomers.^[8f]

The **1a**/*i*PrOH system also showed the highest activity for the ROP of *rac*-MLA^{All} (TOF ≥ 3000 h⁻¹, Table 2, entry 2 vs.

Table 1. Syndiospecific ROP of *rac*-MLA^{Bz} mediated by **1 a–e**/*i*PrOH systems.^[a]

Complex	[MLA ^{Bz}] ₀ /[1] ₀ /[<i>i</i> PrOH] ₀	Reaction time ^[b] [min]	MLA ^{Bz} conv. ^[c] [%]	<i>M</i> _{n,theo} ^[d] [g mol ⁻¹]	<i>M</i> _{n,NMR} ^[e] [g mol ⁻¹]	<i>M</i> _{n,SEC} ^[f] [g mol ⁻¹]	<i>D</i> _M ^[f]	<i>P</i> _r ^[g]	<i>T</i> _m ^[h] [°C]	
1	1 a	25:1:1	1	100	5200	6200	10 600	1.13	0.81	79
2	1 a	50:1:1	1	100	10 400	12 900	19 500	1.08	0.80	74
3	1 a	100:1:1	2	100	20 600	21 000	45 300	1.06	0.79	71
4	1 a	500:1:1	120	0	–	–	–	–	–	–
5	1 a	100:1:0	10	100	20 600	NO ^[i]	41 100	1.23	0.80	72
6 ^[j]	1 a	100:1:0	24 h	0	–	–	–	–	–	–
7	1 b	100:1:1	15	91	18 800	20 300	42 100	1.18	0.85	87
8	1 b	100:1:0	2	100	20 600	NO ^[i]	40 600	1.26	0.85	86
9	1 c	100:1:1	120	96	19 800	19 500	39 200	1.27	0.68	NO ^[i]
10	1 c	100:1:0	120	98	20 200	NO ^[i]	41 200	1.29	0.67	NO ^[i]
11	1 d	50:1:1	75	98	10 100	11 900	22 800	1.45	> 0.95	111
12	1 d	100:1:1	120	80	16 500	17 600	35 200	1.54	> 0.95	117
13	1 d	100:1:0	120	98	20 200	NO ^[i]	37 500	1.44	> 0.95	114
14	1 e	50:1:1	60	100	10 300	11 000	25 000	1.46	0.91	100
15	1 e	100:1:1	120	91	18 800	17 600	35 200	1.54	0.92	104

[a] All reactions were performed with [MLA^{Bz}]₀ = 1.0 M at 20 °C in toluene. [b] Reaction times were not necessarily optimized. [c] MLA^{Bz} conversion as determined by ¹H NMR spectroscopic analysis of the crude reaction mixture. [d] Theoretical molar mass value calculated considering one growing polymer chain per metal center from the relation: *M*_{n,theo} = ([MLA^{Bz}]₀/[*i*PrOH]₀) × conv._{MLABz} × *M*_{MLABz} + *M*_{PrOH} when using *i*PrOH, and ([MLA^{Bz}]₀/[catalyst]₀) × conv._{MLABz} × *M*_{MLABz} in the absence of *i*PrOH, with *M*_{MLABz} = 206 g mol⁻¹ and *M*_{PrOH} = 60 g mol⁻¹. [e] Molar mass value determined by ¹H NMR spectroscopic analysis of the isolated polymer in CDCl₃ at 25 °C, from the resonances of the terminal isopropoxy group. [f] Number-average molar mass value determined by SEC in THF at 30 °C versus polystyrene standards (uncorrected *M*_n values). [g] *P*_r is the probability of racemic linkages between MLA^{Bz} units as determined by ¹³C{¹H} NMR analyses. [h] Melting temperature as determined by DSC (second heating cycle). [i] Not observed. [j] Reaction performed in THF.

Table 2. Syndiospecific ROP of *rac*-MLA^{All} mediated by **1 a–e**/*i*PrOH (1:1) systems.^[a]

Complex	[MLA ^{All}] ₀ /[1] ₀ /[<i>i</i> PrOH] ₀	Reaction time ^[b] [min]	MLA ^{All} conv. ^[c] [%]	<i>M</i> _{n,theo} ^[d] [g mol ⁻¹]	<i>M</i> _{n,NMR} ^[e] [g mol ⁻¹]	<i>M</i> _{n,SEC} ^[f] [g mol ⁻¹]	<i>D</i> _M ^[f]	<i>P</i> _r ^[g]	<i>T</i> _m ^[h] [°C]	
1	1 a	50:1:1	1	100	7900	7500	8900	1.22	0.81	49
2	1 a	100:1:1	2	100	15 700	14 100	29 300	1.03	0.82	51
3	1 b	100:1:1	5	89	14 000	14 600	20 300	1.41	0.87	80
4	1 c	100:1:1	120	100	15 700	15 300	22 100	1.15	0.68	NO ^[i]
5	1 d	100:1:1	10	80	12 500	13 300	23 500	1.64	> 0.95	112
6	1 e	100:1:1	20	100	10 400	9900	19 600	1.54	0.95	107

[a] All reactions were performed with [MLA^{All}]₀ = 1.0 M at 20 °C in toluene. [b] Reaction times were not necessarily optimized. [c] MLA^{All} conversion as determined by ¹H NMR spectroscopic analysis on the crude reaction mixture. [d] Theoretical molar mass value calculated considering one growing polymer chain per metal center from the relation: *M*_{n,theo} = ([MLA^{All}]₀/[*i*PrOH]₀) × conv._{MLAAll} × *M*_{MLAAll} + *M*_{PrOH}, with *M*_{MLAAll} = 156 g mol⁻¹ and *M*_{PrOH} = 60 g mol⁻¹. [e] Molar mass value determined by ¹H NMR spectroscopic analysis of the isolated polymer in CDCl₃ at 25 °C, from the resonances of the terminal isopropoxy group. [f] Number-average molar mass value determined by SEC in THF at 30 °C versus polystyrene standards (uncorrected *M*_n values). [g] *P*_r is the probability of racemic linkages between MLA^{All} units as determined by ¹³C{¹H} NMR analysis. [h] Melting temperature as determined by DSC (second heating cycle). [i] Not observed.

Table 1, entry 3). Lower activities were recorded for systems based on methoxy-capped complexes **1 b**, **1 d**, and **1 e** (generated in situ), although these values were significantly higher in the ROP of *rac*-MLA^{All} than in the ROP of *rac*-MLA^{Bz} (**1 b**: TOF_{MLAAll} = 1100 h⁻¹ vs. TOF_{MLABz} = 360 h⁻¹ (Table 2, entry 3 vs. Table 1, entry 7); **1 d**: TOF_{MLAAll} = 480 h⁻¹ vs. TOF_{MLABz} = 40 h⁻¹ (Table 2, entry 5 vs. Table 1, entry 12); **1 e**: TOF_{MLAAll} ≥ 300 h⁻¹ vs. TOF_{MLABz} = 46 h⁻¹ (Table 2, entry 6 vs. Table 1, entry 15)). The catalyst system based on the bulky **1 c** was clearly the least active in this series. All the PMLA^{All}s synthesized featured experimental molar mass values (*M*_{n,NMR}) in good agreement with theoretical values (*M*_{n,theo}), as well as a monomodal SEC trace and a fairly narrow dispersity (1.03 ≤ *D*_M ≤ 1.64).

The activities of complexes **1 a–c** in the ROP of methyl β-malolactonate significantly surpassed those recorded with *rac*-

MLA^{All} or *rac*-MLA^{Bz} (Table 3 vs. 1, 2, respectively; **1 a**, TOF ≥ 6000 h⁻¹, Table 3, entry 2; **1 b**, TOF ≥ 6000 h⁻¹, Table 3, entry 3; **1 c**, TOF ≥ 1200 h⁻¹, Table 1, entry 4). On the other hand, an opposite trend was observed with halogen-substituted complexes **1 d–e**, for which complete conversion of MLA^{Me} was reached within 48 h, whereas only ca. 20–120 min were necessary with *rac*-MLA^{All} and *rac*-MLA^{Bz}, respectively. Note however that, in contrast to **1 a–c**, complexes **1 d–e** gave insoluble PMLA^{Me}s (suggesting the formation of a highly crystalline polymer, see below), thus affecting the reaction medium and possibly also the reaction kinetics.

Complex	[MLA ^{Me}] ₀ /[1] ₀ / <i>i</i> PrOH ₀	Reaction time ^[b] [min]	MLA ^{Me} conv. ^[c] [%]	<i>M</i> _{n,theo} ^[d] [g mol ⁻¹]	<i>M</i> _{n,NMR} ^[e] [g mol ⁻¹]	<i>M</i> _{n,SEC} ^[f] [g mol ⁻¹]	<i>D</i> _M ^[f]	<i>P</i> _{rr} ^[g]	<i>T</i> _m ^[h] [°C]	
1	1 a	50:1:1	0.5	75	5000	4700	7000	1.15	0.81	173
2	1 a	100:1:1	1	100	13000	17100	24200	1.22	0.76	60
3	1 b	100:1:1	1	100	13000	13100	18400	1.20	0.77	62
4	1 c	100:1:1	5	100	13000	13700	18800	1.24	0.42	NO ^[j]
5 ^[i]	1 d	100:1:1	48 h	100 ^[k]	13000	NO ^[j]	NO ^[j]	NO ^[j]	0.89	207
6 ^[j]	1 e	100:1:1	48 h	100 ^[k]	13000	NO ^[j]	NO ^[j]	NO ^[j]	0.92	212

[a] All reactions were performed with [MLA^M]₀ = 1.0 M at 20 °C in toluene. [b] Reaction times were not necessarily optimized. [c] MLA^{Me} conversion as determined by ¹H NMR spectroscopic analysis of the crude reaction mixture. [d] Theoretical molar mass calculated considering one growing polymer chain per metal center from the relation: *M*_{n,theo} = ([MLA^{Me}]₀/[catalyst]₀ × *M*_{MLA^{Me}}) + *M*_{*i*PrOH}, with *M*_{MLA^{Me}} = 132 g mol⁻¹ and *M*_{*i*PrOH} = 60 g mol⁻¹. [e] Molar mass value determined by ¹H NMR spectroscopic analysis of the isolated polymer in CDCl₃ at 25 °C, from the resonances of terminal isopropoxy group. [f] Number-average molar mass value determined by SEC in THF at 30 °C versus polystyrene standards (uncorrected *M*_n values). [g] *P*_{rr} is the probability of racemic linkages between MLA^{Me} units consecutive to a racemic diad as determined by ¹³C{¹H} NMR spectroscopic analysis and DSC. [h] Melting temperature as determined by DSC (second heating cycle). [i] Not observed. [j] Insoluble polymer. [k] No presence of residual monomer was observed in the soluble fraction.

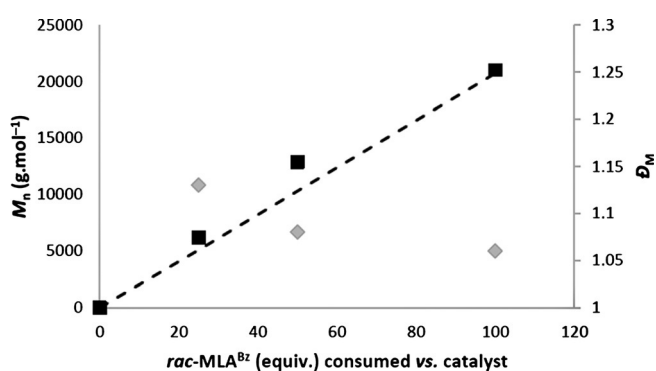


Figure 1. Variation of *M*_{n,NMR} (■), *M*_{n,theo} (dashed line) and *D*_M (◆) of PMLA^{Bz}s synthesized by ROP of *rac*-MLA^{Bz} in the presence of the **1 a**/*i*PrOH (1:1) system (generated in situ), as a function of MLA^{Bz} conversion (Table 1, entries 1–3).

Characterization of PMLA^Rs synthesized by ROP of *rac*-MLA^Rs promoted by **1 a–e**/*i*PrOH systems

All the PHAs synthesized were characterized by ¹H and ¹³C{¹H} NMR spectroscopy and MALDI-ToF mass spectrometry (Figures 2–7). The ¹H NMR spectra of the PMLA^Rs clearly showed signals corresponding to both the MLA^R repeating unit (see the Experimental section) and chain-end groups (Figure 2, Figures 4, 5). Hence, when *i*PrOH was used as co-initiator, all the polymers isolated showed signals for the terminal isopropoxycarbonyl hydrogen atoms (-OCH(CH₃)₂ and -OCH(CH₃)₂ at δ = 4.40–3.40 and 1.30–1.15 ppm, respectively). The ¹³C{¹H} NMR analyses confirmed the nature of the backbone and end-capping groups of PMLA^Rs (Figures 3, S5, S6 and S8 for PMLA^{All}, PMLA^{Bz} and PMLA^{Me}, respectively).

The chemical structure of PMLA^Rs was further supported by MALDI-ToF MS analyses. The spectra recorded from a low molar mass sample of PMLA^{Bz} prepared with the **1 a**/*i*PrOH system revealed two populations of macromolecules, both featuring a repeating unit of *m/z* 206 g mol⁻¹ (*M*_{MLA^{Bz}}). The first corresponds to the anticipated α-isopropoxy,ω-hydroxyl and α-isopropoxy,ω-dehydrated (i.e., crotonate) PMLA^{Bz} chains both ionized by

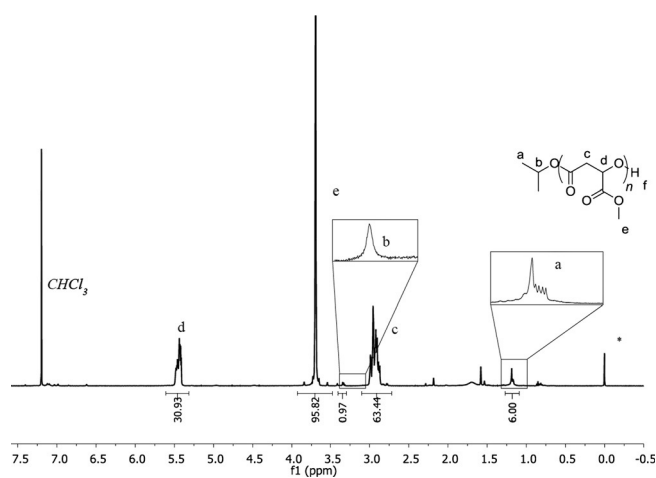


Figure 2. ¹H NMR spectrum (500 MHz, CDCl₃, 25 °C) of a PMLA^{Me} prepared from the ROP of *rac*-MLA^{Me} mediated by complex **1 a** in the presence of 1 equiv of *i*PrOH (Table 3, entry 1; *: signal from residual grease).

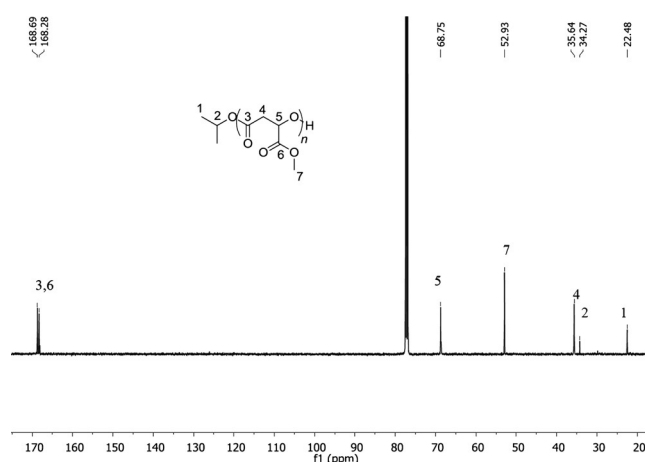


Figure 3. ¹³C{¹H} NMR spectrum (125 MHz, CDCl₃, 25 °C) of a PMLA^{Me} prepared by ROP of *rac*-MLA^{Me} with **1 a** in the presence of 1 equiv of *i*PrOH (Table 3, entry 1).

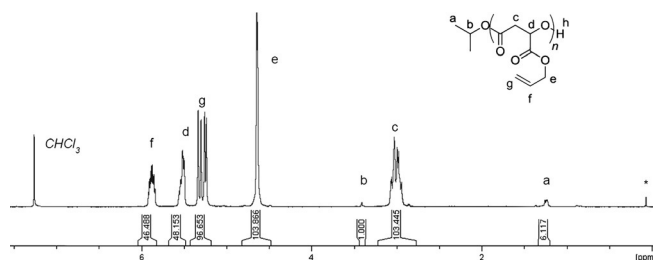


Figure 4. ^1H NMR spectrum (500 MHz, CDCl_3 , 25°C) of a PMLA^{All} prepared from the ROP of $\text{rac-MLA}^{\text{All}}$ mediated by complex **1a** in the presence of 1 equiv of *i*PrOH (Table 2, entry 1; *: signal from residual grease).

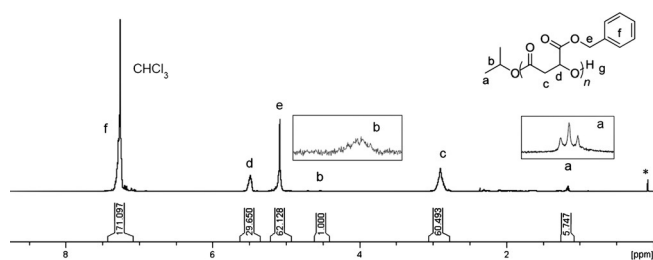


Figure 5. ^1H NMR spectrum (500 MHz, CDCl_3 , 25°C) of a PMLA^{Bz} prepared from the ROP of $\text{rac-MLA}^{\text{Bz}}$ mediated by complex **1a** in the presence of 1 equiv of *i*PrOH (Table 1, entry 1; $M_{n,\text{NMR}} = 6200 \text{ g mol}^{-1}$; *: signal from residual grease).

Na^+ (Figure 6). This was unequivocally confirmed by the close match with the isotopic simulations for $[(\text{CH}_3)_2\text{CH}(\text{COCH}_2\text{CH}(\text{COOCH}_2\text{C}_6\text{H}_5)\text{O})_n\text{H}]\cdot\text{Na}^+$ with, for example, calculated m/z $4206.2 \text{ g mol}^{-1}$ versus found m/z $4205.7 \text{ g mol}^{-1}$ for $n=20$, and $[(\text{CH}_3)_2\text{CH}(\text{COCH}_2\text{CH}(\text{COOCH}_2\text{C}_6\text{H}_5)\text{O})_n\text{H}-\text{H}_2\text{O}]\cdot\text{Na}^+$ with, for example, calculated m/z $4188.2 \text{ g mol}^{-1}$ versus found m/z $4188.7 \text{ g mol}^{-1}$ for $n=20$ (expansion of Figure 6). The second population corresponds to α -amido, ω -hydroxy and α -amido, ω -dehydrated PMLA^{Bz} chains, both ionized by H^+ (see Figure S7). The presence of this latter population reflects the occurrence of amido-initiation, likely due to the use of a slight default of isopropanol versus the amido precursor; however, the good agreement between theoretical ($M_{n,\text{theo}}$) and experimental ($M_{n,\text{NMR}}$) molar mass values of PMLA^{Bz} s determined from the isopropoxycarbonyl terminal group indicates that amido-initiation remained minimal versus isopropoxide-initiation and suggests that the latter macromolecules may be overexpressed in these MALDI-TOF MS analyses. In fact, the MALDI-ToF mass spectrum of a low molar mass PMLA^{All} sample synthesized with the same **1a**/*i*PrOH catalytic system displayed a unique population of macromolecules with a repeating unit of m/z 156 g mol^{-1} ($M_{\text{MLA}^{\text{All}}}$; Figure 7), assigned to α -isopropoxy, ω -hydroxy or α -isopropoxy, ω -dehydrated (i.e., crotonate) PMLA^{All} chains ionized by Na^+ ; namely, $[(\text{CH}_3)_2\text{CH}(\text{COCH}_2\text{CH}(\text{COOCH}_2\text{CH}_2\text{O})_n\text{H})]\cdot\text{Na}^+$ with, for example, calculated m/z $2424.7 \text{ g mol}^{-1}$ (vs. found m/z $2424.4 \text{ g mol}^{-1}$) and $[(\text{CH}_3)_2\text{CH}(\text{COCH}_2\text{CH}(\text{COOCH}_2\text{CH}_2\text{O})_n\text{H}-\text{H}_2\text{O})]\cdot\text{Na}^+$ with, for example, calculated m/z $2406.7 \text{ g mol}^{-1}$ versus found m/z $2406.4 \text{ g mol}^{-1}$ for $n=15$, as confirmed by the isotopic simulations (expansion, Figure 7). The absence of noticeable crotonate groups in the NMR spectra of the prepared PMLA^{Bz} and PMLA^{All}

suggests that dehydration of the macromolecular chains occurs during the MALDI-ToF MS analyses.

Microstructural analysis and syndiotactic enrichment of PMLA^{R} s

Well-defined PMLA^{R} s were synthesized by ROP of $\text{rac-MLA}^{\text{R}}$ s by using complexes **1a–e** and *i*PrOH as co-initiator. The latter yttrium catalysts are known to be stereoselective for the ROP of $\text{rac-}\beta$ -butyrolactone as well as of rac-lactide .^[6a,8a,d,13] To confirm the microstructure of the PMLA^{R} s synthesized in the present work, $^{13}\text{C}\{^1\text{H}\}$ NMR analyses were carried out. The methine region of the $^{13}\text{C}\{^1\text{H}\}$ NMR spectra of PMLA^{Bz} and PMLA^{All} revealed four signals corresponding to triad stereosequences; namely, *racemo-racemo* (*rr*), *meso-racemo* (*mr*), *racemo-meso* (*rm*) and *meso-meso* (*mm*) (Figures 8 and 9, respectively). Assignment of signals in this region was performed based on previous work on stereoenriched PMLA^{Bz} ,^[14] stereocopolymers,^[15] as well as by comparison with isotactic and atactic PMLA^{Bz} s synthesized from the ROP of (*R*)- MLA^{Bz} and $\text{rac-MLA}^{\text{Bz}}$ by using $[(\text{BDI})\text{Zn}\{\text{N}(\text{SiMe}_3)_2\}]/i\text{PrOH}$ (1:1) as catalytic system, respectively (Figure 8a).^[16,17] Four triads were thus observed for PMLA^{Bz} s ($\delta = 68.70 \text{ ppm}$, *rr*; $\delta = 68.61 \text{ ppm}$, *mr*; $\delta = 68.53 \text{ ppm}$, *rm*; $\delta = 68.42 \text{ ppm}$, *mm*; Figure 8 b), and PMLA^{All} s ($\delta = 68.79 \text{ ppm}$, *rr*; $\delta = 68.70 \text{ ppm}$, *mr*; $\delta = 68.68 \text{ ppm}$, *rm*; $\delta = 68.61 \text{ ppm}$, *mm*; Figure 9). The larger contribution of the *rr* triad, compared with the much smaller ones of the *mr*, *rm* and *mm* triads, thus supported the predominant syndiotacticity of the PMLA^{R} s ($\text{R} = \text{All}$, Bz) formed.

The syndiotactic enrichment of PMLA^{Bz} s and PMLA^{All} s was determined by calculating the probability of racemic linkage (P_r) through a statistical analysis of the triad distribution. The methine signals were deconvoluted with the aim to compare the relative integration value of each triad signal (Figure 10). A first-order chain-end control (or Markov first-order chain-end control, Mk1) is defined in terms of probability of a racemic (P_r) or meso (P_m) linkage.^[18] By comparing these predicted values to those observed in the NMR spectra, the mechanism of stereocontrol and the degree of stereoselectivity in the polymerization can be determined. For triad stereosequences, the agreement with an Mk1 mechanism was supported by the calculation of a Bernoullian test factor ($B = 4(mm)(rr)/[(mr) + (rm)]$), which was close to unity for a perfect first-order chain-end control. In fact, the latter factors corresponding to the synthesized PMLA^{Bz} s and PMLA^{All} s were close to unity ($1.02 \leq B \leq 1.34$; Tables S1 and S2), confirming the good agreement with the Mk1 chain-end mechanism. Analyses of the relative contributions of the different stereosequences confirmed a Mk1-type stereocontrol mechanism,^[18] as reported for rac-lactide and $\text{rac-}\beta$ -butyrolactone.^[6a,8a,d,13]

Microstructural analysis of PMLA^{Me} proved to be somewhat more challenging than that of PMLA^{Bz} and PMLA^{All} . Indeed, tetrad stereosequences were observed in the methine region of the $^{13}\text{C}\{^1\text{H}\}$ NMR spectrum of PMLA^{Me} ($\delta = 68.78 \text{ ppm}$; *rrr*, $\delta = 68.75 \text{ ppm}$; *rrm*, $\delta = 68.71 \text{ ppm}$; *rrm*, $\delta = 68.67 \text{ ppm}$; *mrr*, $\delta = 68.64 \text{ ppm}$; *rrm*, $\delta = 68.61 \text{ ppm}$; *mmm*, $\delta = 68.58 \text{ ppm}$; *mrm*, $\delta = 68.56 \text{ ppm}$) (Figure 11). These signals were assigned

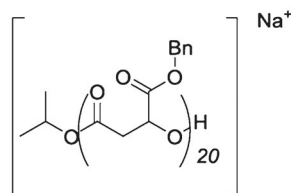
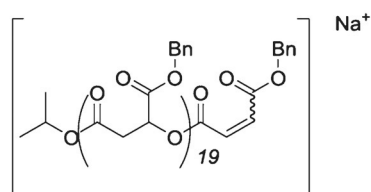
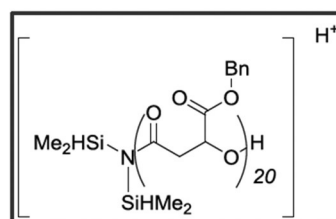
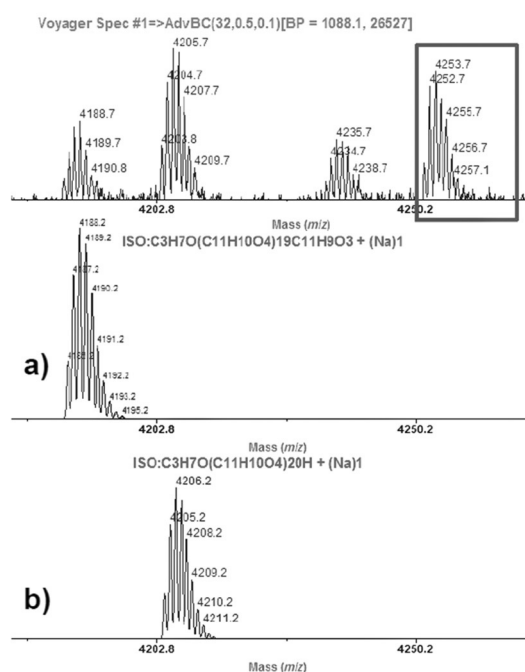
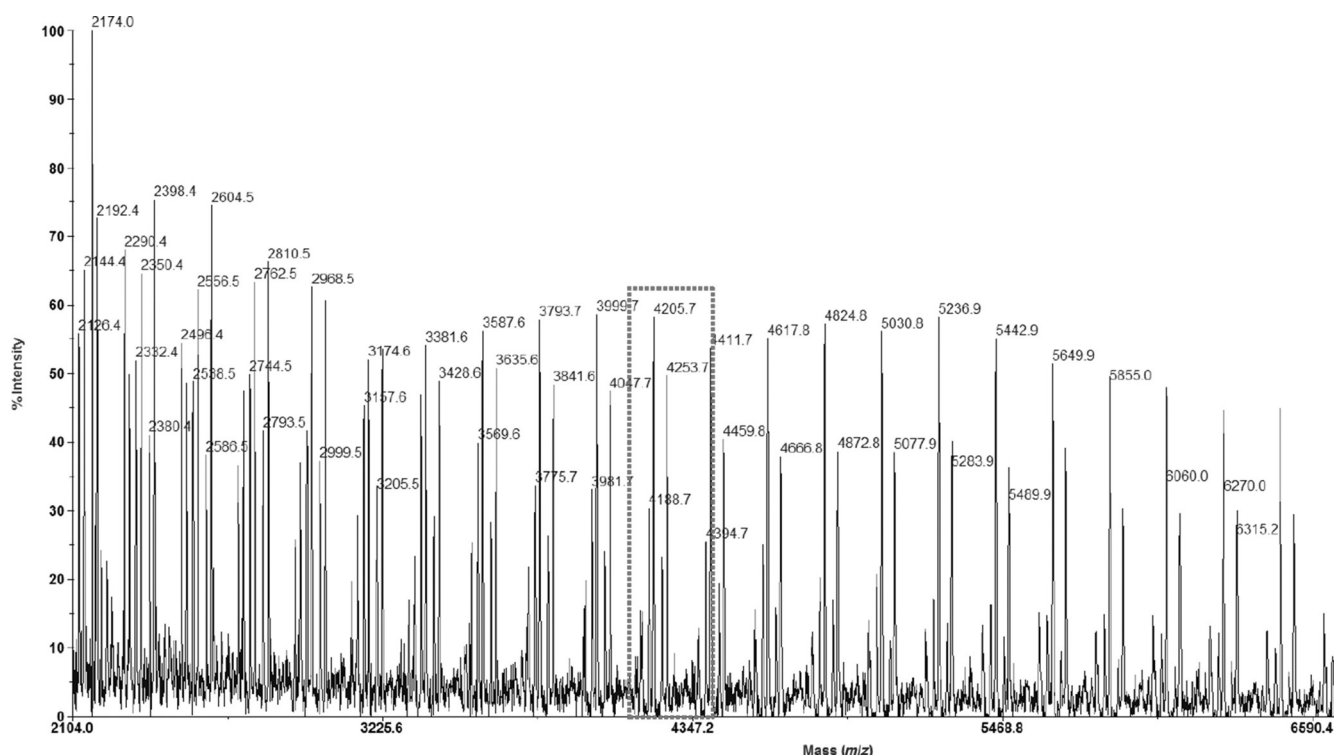
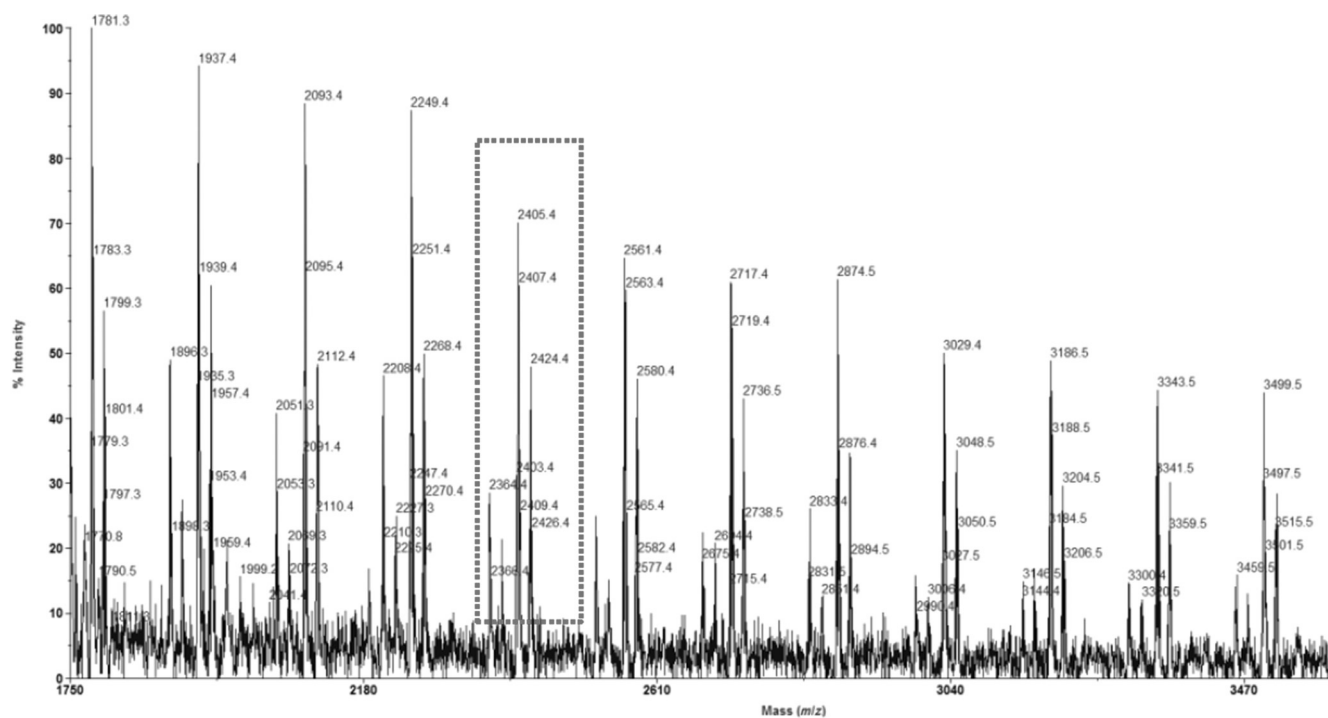


Figure 6. MALDI-ToF mass spectrum (matrix IAA) of a PMLA^{Bz} prepared from the ROP of *rac*-MLA^{Bz} mediated by the **1 a**/iPrOH system (Table 1, entry 2). The major population stands for [iPrO{MLA^{Bz}]_nH]·Na⁺ macromolecules (refer to simulation **b** for *n* = 20). The minor population stands for [iPrO{MLA^{Bz}]_nH–H₂O]·Na⁺ macromolecules (refer to simulation **a** for *n* = 20). Secondary populations stand for [(SiHMe₂)₂N{MLA^{Bz}]_nH]·H⁺ and [(SiHMe₂)₂N{MLA^{Bz}]_nH–H₂O]·H⁺.

by comparison with isotactic PMLA^{Me}, for which only the *mmm* tetrad was observed (Figure 11, isotactic), along with statistical analysis. The major contribution of the *rrr* tetrad for the PMLA^{Me}s synthesized by ROP of *rac*-MLA^{Me} in the presence of **1 a–c**/iPrOH systems supported the high syndiotacticity of this material.

By analogy with the formation of syndiotactic PMLA^{Bz} and PMLA^{All}, the stereocontrol in the ROP of MLA^{Me} was expected to take place through a chain-end control mechanism. Unfortunately, for tetrad stereosequences, the validity of this hypothesis could not be verified from the calculation of a Bernoullian test factor. Two statistic models were then investigat-



#1=>AdvBC(32.0,5,0.1)[BP = 1088.1, 9370]

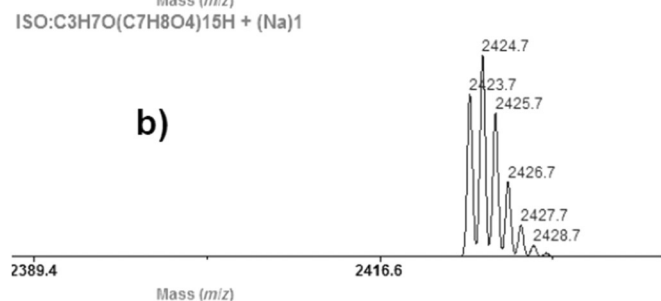
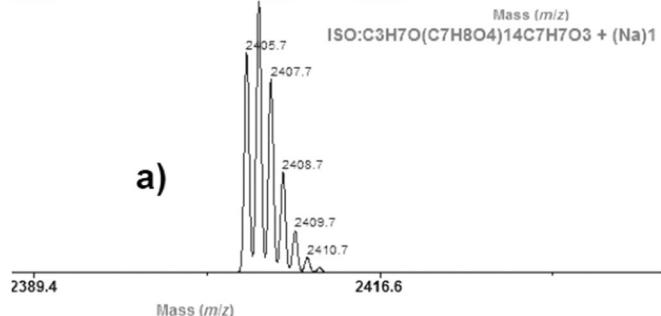
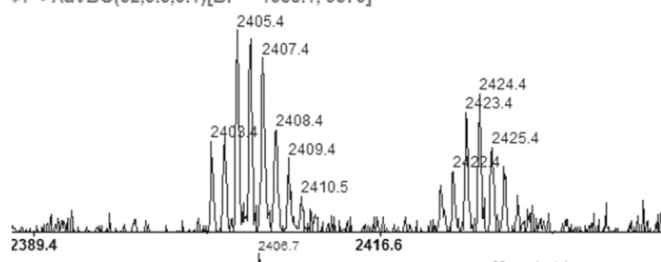


Figure 7. MALDI-ToF mass spectrum (matrix IAA) of a PMLA^{All} prepared from the ROP of *rac*-MLA^{All} mediated by the 1 a/*i*PrOH system (Table 2, entry 1). The major population stands for [*i*PrO(MLA^{All})_nH–H₂O]·Na⁺ macromolecules (refer to simulation **a** for *n* = 15). The minor population stands for [*i*PrO(MLA^{All})_nH]·Na⁺ macromolecules (refer to simulation **b** for *n* = 15).

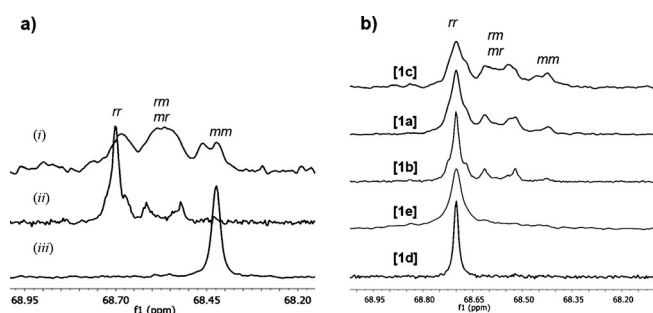


Figure 8. Detail of the methine region of the $^{13}\text{C}\{^1\text{H}\}$ NMR spectra (125 MHz, CDCl_3 , 25°C) of PMLA^{Bz}s synthesized from ROP of *rac*-MLA^{Bz} in the presence of a) (i) [(BDI)Zn(N(SiMe₃)₂)]/*i*PrOH system ($P_r = P_m = 0.5$); (ii) **1 b**/*i*PrOH ($P_r = 0.85$; Table 1, entry 7); (iii) [(BDI)Zn(N(SiMe₃)₂)]/*i*PrOH system ($P_m > 0.95$); and b) **1 c**/*i*PrOH ($P_r = 0.68$; Table 1, entry 9); **1 a**/*i*PrOH ($P_r = 0.79$; Table 1, entry 3); **1 b**/*i*PrOH ($P_r = 0.85$; Table 1, entry 7); **1 e** (in situ generated)/*i*PrOH ($P_r = 0.92$; Table 1, entry 15); **1 d**/*i*PrOH ($P_r > 0.95$; Table 1, entry 11).

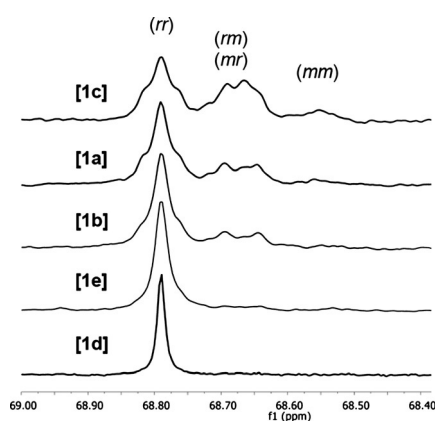


Figure 9. Detail of the methine region of the $^{13}\text{C}\{^1\text{H}\}$ NMR spectra (125 MHz, CDCl_3 , 25°C) of PMLA^{AlI}s synthesized from ROP of *rac*-MLA^{AlI} in the presence of the **1 c**/*i*PrOH system ($P_r = 0.68$; Table 2, entry 4); **1 a**/*i*PrOH ($P_r = 0.82$; Table 2, entry 2); **1 b**/*i*PrOH ($P_r = 0.87$; Table 2, entry 3); **1 e** (in situ generated)/*i*PrOH ($P_r = 0.95$; Table 2, entry 6); **1 d**/*i*PrOH ($P_r > 0.95$; Table 2, entry 5).

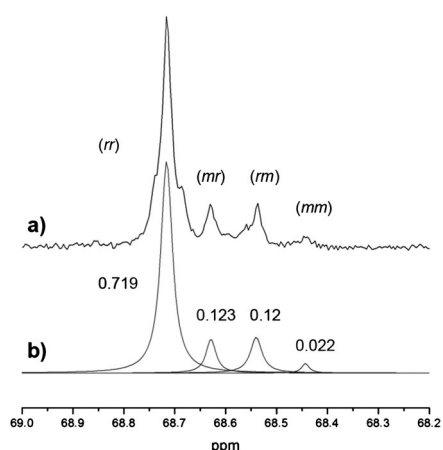


Figure 10. a) Methine region of the $^{13}\text{C}\{^1\text{H}\}$ NMR spectrum (125 MHz; CDCl_3 ; 25°C) of a PMLA^{Bz} prepared from the ROP of *rac*-MLA^{Bz} mediated by the **1 b**/*i*PrOH system ($P_r = 0.85$; Table 1, entry 7); b) Lorentzian deconvolution of the methine region^[19] (values of integrals corresponding to deconvoluted signals). The P_r value was calculated from the following equation: $P_r = \sqrt{(r)}$.^[18]

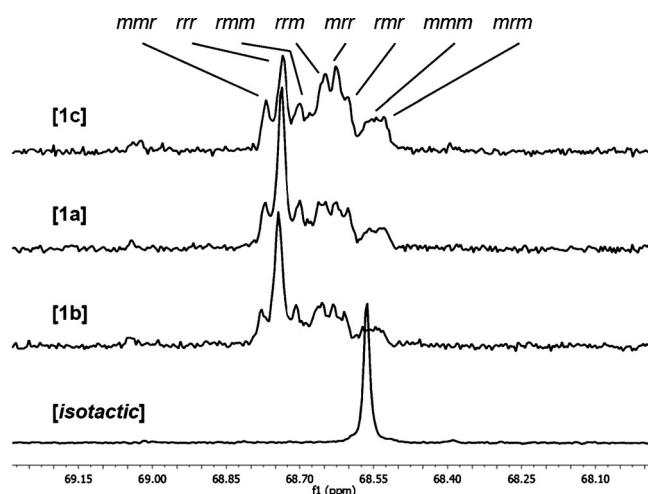


Figure 11. Detail of the methine region of the $^{13}\text{C}\{^1\text{H}\}$ NMR spectra (125 MHz, CDCl_3 , 25°C) of PMLA^{Me}s synthesized from ROP of *rac*-MLA^{Me} in the presence of the **1 c**/*i*PrOH system ($P_{r/r} = 0.43$; Table 3, entry 4); **1 a**/*i*PrOH ($P_{r/r} = 0.76$; Table 3, entry 2); **1 b**/*i*PrOH ($P_{r/r} = 0.77$; Table 3, entry 3); ROP of (*R*)-MLA^{Me} mediated by **1 a** ($P_m > 0.95$).

ed for the analysis of the stereocontrol mechanism, namely Markov first-order (Mk1) and Markov second-order (Mk2) models.^[18] These latter models fit with a chain-end control driven by the last and the penultimate repeating units of the growing-chain, respectively. The tetrads contribution were evaluated by deconvolution of the NMR massif corresponding to the methine region of the $^{13}\text{C}\{^1\text{H}\}$ NMR spectrum ($\delta = 68.5$ – 69.0 ppm), as illustrated in Figure 12, according to a previously reported approach.^[3]

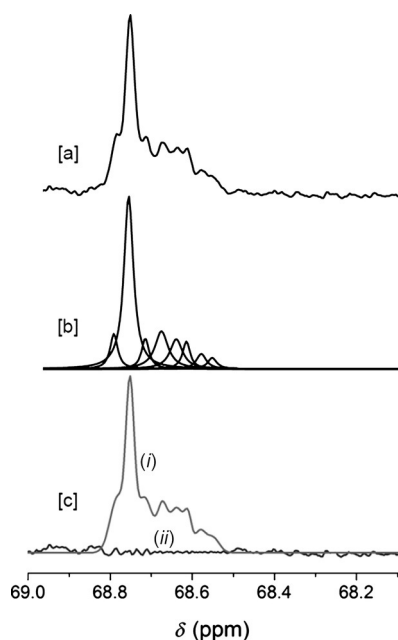


Figure 12. Deconvolution of the signals of the methine region of the $^{13}\text{C}\{^1\text{H}\}$ NMR spectrum (125 MHz, CDCl_3 , 25°C) of PMLA^{Me} prepared from the ROP of *rac*-MLA^{Me} mediated by the **1 a**/*i*PrOH system (Table 3, entry 1) using Lorentz functions.^[16] [a] Observed spectrum; [b] Eight-component signal resolved; and [c] (i) simulated spectrum using the component peaks in [b], and (ii) differential spectrum obtained upon subtracting [c] from [a].

The experimental data were then fitted with the theoretical values obtained by using the Mk1 and Mk2 models (Figure 13). Although both models afforded good agreement between experimental and theoretical contributions of the *rrr* tetrad, the Mk2 model afforded a much better agreement for all the seven other tetrads' contribution. The statistical analysis fitting data for PMLA^{Me}s are reported in Table 4, whereas the data for statistical analyses for other PMLA^Rs are gathered in the Supporting Information (Tables S3–S6). The stereocontrol was found to be of Mk2 type, indicating that the last two inserted repeating units of the growing-chain directly impact the insertion of the next monomer.

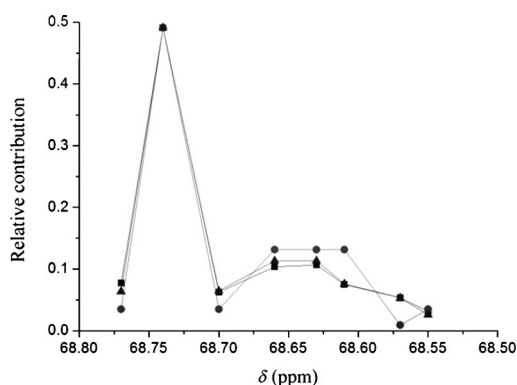


Figure 13. Fitting of the statistical repartition obtained by experiment (■), first-order Markov model (●; RMS error = $3.36 \cdot 10^{-2}$) and second-order Markov model (▲; RMS error = $0.67 \cdot 10^{-2}$) for a PMLA^{Me} synthesized from the ROP of *rac*-MLA^{Me} mediated by the **1 a**/iPrOH system (Table 3, entry 1).

Entry	Complex	Markov 1st order Fitting with experiment (RMS error) ^[20]	P_r	Markov 2nd order Fitting with experiment (RMS error) ^[20]	P_{rr}
1	1 a	3.36×10^{-2}	0.79	0.67×10^{-2}	0.81
2	1 a	4.16×10^{-2}	0.75	3.33×10^{-2}	0.76
3	1 b	5.43×10^{-2}	0.74	4.53×10^{-2}	0.77
4	1 c	3.88×10^{-2}	0.59	3.72×10^{-2}	0.60

[a] Mk1 and Mk2 statistical models used as defined by Sepulchre for the ROP of a lactone containing only one asymmetric center.^[18]

The syndioselectivity of yttrium complexes **1 a–e** was then evaluated by a statistical treatment of the contribution of the different triads observed from the methine region of ¹³C{¹H} NMR spectra of the resulting PMLA^Rs, using Markov first-order model (Mk1) for PMLA^{Bz} and PMLA^{All}, and the contribution of the different tetrads, using Markov second-order model (Mk2) for PMLA^{Me} (see above).^[18] These latter treatments allowed the probability of racemic linkage (P_r) for PMLA^{Bz} and PMLA^{All}, and the probability of linkages between MLA^{Me} units consecutive to a racemic diad (P_{rr}) for PMLA^{Me} to be calculated.

A consistent trend in stereoselectivity was hence observed for the ROP of MLA^{Bz} and MLA^{All} mediated by complexes **1 a–e**. First, the highest stereoselectivities were measured for catalysts with halogen-disubstituted ligands; that is, **1 d** ($P_r > 0.95$; Table 1, entries 11–13 and Table 2, entry 5, for PMLA^{Bz} and PMLA^{All}, respectively) and **1 e** ($P_r = 0.91–0.95$; Table 1, entries 14–15 and Table 2, entry 6, for PMLA^{Bz} and PMLA^{All}, respectively). The syndiotactic enrichment induced by catalysts **1 a** ($P_r = 0.79–0.81$; Table 1, entries 1–5 and Table 2, entries 1–2, for PMLA^{Bz} and PMLA^{All}, respectively) and **1 b** ($P_r = 0.85–0.87$; Table 1, entries 7–8 and Table 2, entry 3, for PMLA^{Bz} and PMLA^{All}, respectively) remained more modest. A more significant decrease of the stereocontrol was calculated for **1 c** ($P_r = 0.67–0.68$; Table 1, entries 9–10 and Table 2, entry 4, for PMLA^{Bz} and PMLA^{All}, respectively). The Mk2 model allowed the measurement of syndiotactic enrichment of soluble PMLA^{Me}s synthesized from **1 a–c**. The trend observed for the other two PMLA^Rs (R = Bz, All) was similarly observed in the ROP of *rac*-MLA^{Me}. Indeed, catalyst **1 c** ($P_{rr} = 0.60$; Table 3, entry 4) showed a lower enrichment than **1 b** ($P_{rr} = 0.77$; Table 3, entry 3) and **1 a** ($P_{rr} = 0.76–0.81$; Table 3, entries 1–2). The PMLA^{Me}s synthesized with complexes with halogen-disubstituted ligands **1 d–e** proved to be very poorly soluble in common organic solvents. This insolubility hinted at highly crystalline samples, likely arising from the high regularity of the stereosequences in the polymer chain. The syndiotactic enrichment of these PMLA^{Me}s was further estimated by DSC thermal analysis (see below). In this case, **1 e** ($P_{rr} \approx 0.92$; Table 3, entry 6) proved to be slightly most selective than **1 d** ($P_{rr} \approx 0.89$; Table 3, entry 5).

These results, similar to those previously reported in the ROP of *rac*-BL and *rac*-LA,^[8d,13] point out the key influence of the *ortho*-substituents of the amino-alkoxy-bis(phenolate) ligand on the stereoselectivity of complexes **1 a–e**.^[10] Nevertheless, the relationship between the nature of the *ortho*-substituent and the stereoselectivity is completely different in the case of the *rac*-MLA^{Bz}s: R¹ = CPh₃ (**1 c**; $P_r = 0.68$) < CMe₂Ph (**1 a**; $P_r = 0.79$) < CMe₂tBu (**1 b**; $P_r = 0.85$) ≪ Cl (**1 d**; $P_r > 0.95$), than the trends observed with *rac*-LA: R¹ = Cl ($P_r = 0.56$) < CMe₂Ph ($P_r = 0.90$) < CMe₂tBu ($P_r = 0.94–0.95$) < CPh₃ ($P_r = 0.95–0.96$).^[8d] and *rac*-BL: R¹ = Cl ($P_r = 0.42–0.45$) < CMe₂tBu ($P_r = 0.62–0.70$) < CMe₂Ph ($P_r = 0.94–0.95$) < CPh₃ ($P_r = 0.94$).^[8d] These differences are more significant with the bulky and aromatic substituents CMe₂Ph or CPh₃ ($P_{r/rac-LA} = 0.90$ and 0.96 ; $P_{r/rac-BL} = 0.89$ and 0.94 , versus $P_{r/rac-MLA}^{Bz} = 0.79$ and 0.68 , respectively). On the other hand, catalysts incorporating Cl substituents gave a poor selectivity towards *rac*-LA and *rac*-BL,^[8d] whereas this behavior is reversed in the case of *rac*-MLA^Rs ($P_{r/rac-LA} = 0.56$; $P_{r/rac-BL} = 0.42$, vs. $P_{r/rac-MLA}^R > 0.95$).

Although quite seldom seen in the literature, highly stereoselective aluminum complexes bearing halogen-disubstituted salan and salen complexes have been reported for the ROP of *rac*-LA by Gibson et al.^[21] The exact role of the halogen substituent in the stereocontrol ability of these systems remains unclear, but electronic contributions to the stereochemistry of insertion were suggested.^[21] In previous investigations on syndioselective ROP of simple β-lactones such as BL, based on the pioneering work of Rzepa et al. in the ROP of lactide,^[22] we

also pinpointed electronic contributions, namely C–H... π (arene) interactions involving the acidic methylene hydrogen atoms of the κ^2 -*O,O*- β -alkoxybutyrate-type propagating chain and the aryl rings present on *ortho*-substituents of the phenolate moieties of the ligands.^[8d] This accounted for the clear superiority of CMe₂Ph- and CPh₃- *ortho*-substituted systems towards similarly sterically crowded but purely aliphatic versions such as the CMe₂tBu-substituted system. Such stabilizing C–H... π (arene) interactions (estimated as ca. 5–10 kcal mol⁻¹) were supported by DFT computations performed on model species.^[8d]

The above model is clearly unsatisfactory for the present ROP of β -malolactonates, because both CPh₂Me- (**1a**) and CPh₃- (**1c**)-substituted systems gave poor syndioselectivities. We therefore explored the possible involvement of C–X...O=C halogen bonding^[23,24] between *ortho*-halogen substituents and oxygen from carbonyl/alkoxy groups of the propagating poly-(alkoxybutyrate) chain. For this purpose, DFT computations were performed on an yttrium species bearing an allyl β -alkoxybutyrate moiety as a model of the propagating chain. Mononuclear and dinuclear geometries,¹ varying in the positioning of the κ^2 -coordinated *O,O*- β -alkoxybutyrate moiety were explored (Figure 14). However, all of the mononuclear species fell into a narrow range of energies, and in none of these were any close contacts (<3 Å) between the allyl β -alkoxybutyrate and Cl moieties detected. For the computed dinuclear species, such close contacts could be detected but only in structures of significantly higher relative energies (>8.6 kcal mol⁻¹). Similar geometries and relative energies were also computed for similar models bearing CMe₂Ph instead of Cl substituents (see Table S7). Overall, these non-exhaustive DFT computations suggest that halogen bonding is likely not at the origin of the high stereocontrol featured by systems **1d** and **1e**. Initially, the dibromo-substituted complex **1e** was designed to explore experimentally the influence of the halogen substituent on the stereoselectivity, by comparison with the dichloro-substituted **1d** system; bromide is clearly bulkier and also more prone to halogen bonding than chloride. As a matter of fact, both **1d** and **1e** systems lead to close stereoselectivities in the ROP of *rac*-MLA^{Bz} and *rac*-MLA^{All}. Given that in the bromo- and chloro-substituted catalyst systems **1d** and **1e** there is a delicate balance between steric and electronic factors, it remains difficult to deduce which is the actual driving phenomenon responsible for the improved stereocontrol provided by these halogen-substituted systems in the ROP of MLA^Rs.

Thermal analysis of the PMLA^Rs

Analysis by differential scanning calorimetry (DSC) of the thermal behavior of the synthesized PMLA^{Bz}s showed, as expected,

¹ Complex **1d** is dinuclear in the solid state, as established by X-ray diffraction studies. In toluene or benzene solutions, complexes **1d** and **1e** feature a complex NMR behavior and well-resolved, informative spectra could be obtained at low temperature (see the Supporting Information Figure S9 for **1d**). DOSY NMR spectroscopic analysis for **1d** in [D₆]toluene at room temperature (that is, under the same conditions as those used for polymerizations) was consistent with a mononuclear structure (see the Supporting Information).

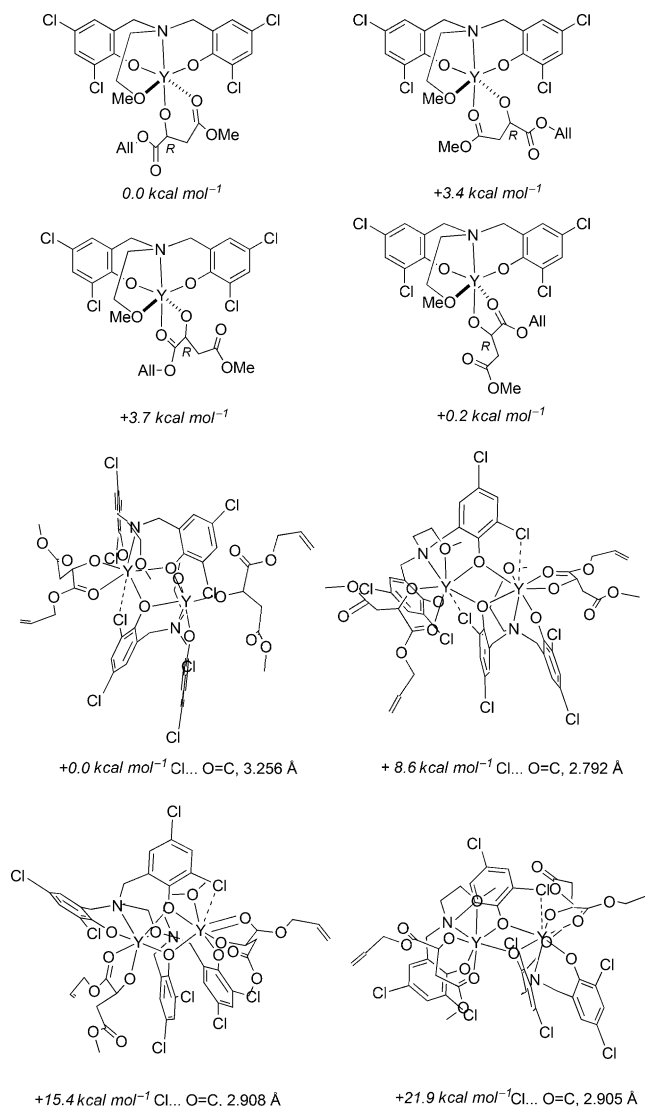


Figure 14. Schematic representation of model mononuclear (top) and dinuclear (bottom) intermediates in the ROP of *rac*-MLA^{All} mediated by [Y(ONOO^{Cl2})] complexes used for DFT computations (BP86-RI/def-TZVP), showing the different arrangements of the κ^2 -coordinated *O,O*- β -alkoxybutyrate moiety investigated and relative computed energies (see the Supporting Information).

a strong influence of the stereoregulation on the melting temperature (T_m ; Table 1). The T_m values increased with P_r values from $T_m = 71^\circ\text{C}$ for $P_r = 0.79$ up to $T_m = 117^\circ\text{C}$ for $P_r > 0.95$ (Figure S9; Table 1, entry 12). A melting transition was observed only for the most stereoregular PMLA^{Bz}s ($P_r \geq 0.79$), illustrating the close stereoregularity/semicrystallinity relationship. The melting temperature of highly syndiotactic-enriched PMLA^{Bz}s ($T_m = 114\text{--}117^\circ\text{C}$) remained significantly lower than that of isotactic PMLA^{Bz}s ($T_m = 180\text{--}190^\circ\text{C}$).^[15,25] All the PMLA^{Bz}s showed a glass-transition temperature in the range $T_g = 30\text{--}35^\circ\text{C}$.

A similar trend was obtained with PMLA^{All}s. The highest melting temperatures were observed for the most stereoregular polymers, $T_m = 112^\circ\text{C}$ for $P_r > 0.95$ (Figure S10; Table 2, entry 5), whereas no melting temperature was recorded for the

least syndiotactic-enriched PMLA^{All} ($P_{r/r} \leq 0.81$). Melting temperatures were also recorded for PMLA^{Me}s, only for highly syndiotactic-enriched stereosequences ($P_{r/r} > 0.76$), whereas the highest T_m value was reached for insoluble PMLA^{Me}s ($T_m = 212^\circ\text{C}$; Table 3, entry 6). These T_m values of syndiotactic PMLA^{Me}s are higher than those of isotactic PMLA^{Me}s ($T_m = 137\text{--}151^\circ\text{C}$).^[26] In the case of the PMLA^{Me} obtained from complex **1d**, a second minor melting temperature was observed at $T_m = 197^\circ\text{C}$ (Figure 15). The presence of two T_m values may arise from the coexistence of two distinct crystalline phases.^[26] The concomitant increase of both T_m and melting enthalpy values with the $P_{r/r}$ of PMLA^{Me}s synthesized from the ROP of *rac*-MLA^{Me} mediated by complexes **1a–c** was fitted empirically (Table S8). This model allowed the syndiotactic enrichment of insoluble PMLA^{Me}s to be evaluated (Figure S11–S13). $P_{r/r}$ values of 0.89 and 0.92 were thus estimated for the PMLA^{Me}s obtained using complexes **1d** and **1e**, respectively (see above). The validity of these values was verified by the linear correlation of the melting temperature with $P_{r/r}$ values (Figure 16). A glass transition temperature $T_g \approx 40^\circ\text{C}$ was recorded for all PMLA^{Me}s.

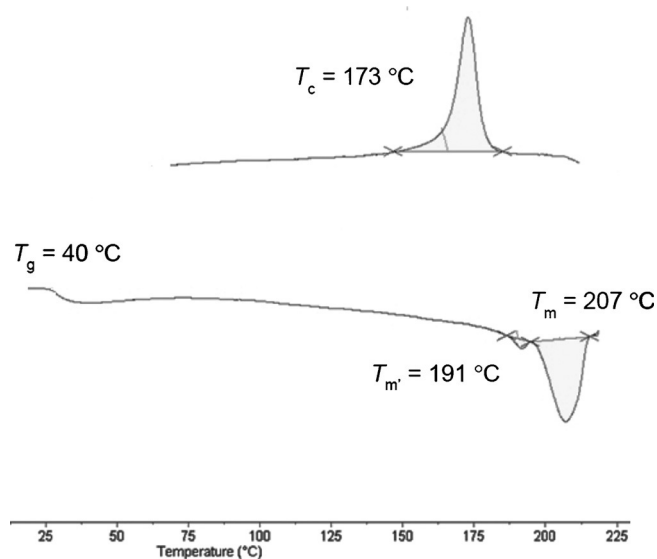


Figure 15. DSC trace (cycle from -50 to 250°C ; 10°Cmin^{-1} ; first heating, $\Delta H_m = 64.1 \text{ J g}^{-1}$) of a PMLA^{Me} obtained from the ROP of *rac*-MLA^{Me} mediated by the **1d**/iPrOH system ($P_{r/r} = 0.89$; Table 3, entry 5).

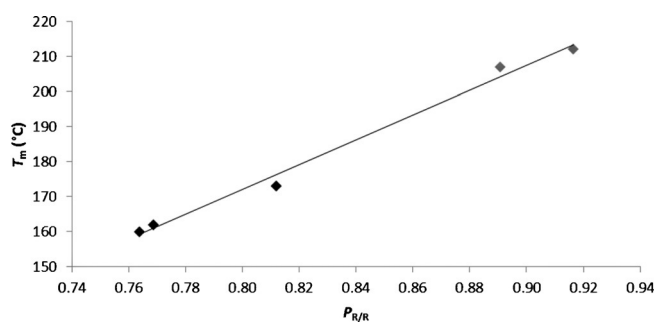


Figure 16. Validation of the estimated $P_{r/r}$ (\blacklozenge) values, obtained by extrapolation of the fitting $\Delta H_m = 7.10^{-6} e^{17.992P_{r/r}}$, by linear correlation of $P_{r/r}$ (\blacklozenge) with T_m values of PMLA^{Me}s synthesized from the ROP of *rac*-MLA^{Me} in the presence of **1a–e**/iPrOH systems (fitting: $y = 354.07x - 111.21$; $R^2 = 0.991$).

Conclusions

Highly syndioselective ROPs of racemic alkyl β -malolactonates (*rac*-MAL^Rs), mediated by [amino-alkoxy-bis(phenolate)]-yttrium amido complexes **1a–e** in the presence of a co-initiator (isopropanol), have been performed. All yttrium complexes were efficient, providing the best activities recorded for this class of monomer ($\text{TOF} \geq 3000 \text{ h}^{-1}$), and afforded well-defined PMLA^Rs ($4700 \text{ g mol}^{-1} \leq M_n \leq 21000 \text{ g mol}^{-1}$) with good control of the polymerization ($D_M \leq 1.55$). In contrast to the ROP of other related monomers, such as *rac*-LA and even *rac*-BL, the yttrium catalysts bearing halogen-disubstituted ligands were the most stereoselective ($P_r \geq 0.95$). Effective chain-end control mechanisms were attributed to Markov first-order mechanism for the ROP of *rac*-MLA^{Bz} and *rac*-MLA^{All}, and to Markov second-order for the ROP of *rac*-MLA^{Me}. The high stereoselectivity achieved with the halogen-substituted catalysts definitively hints at electronic effects, which are clearly of different nature than those pinpointed with *aryl*-substituted catalysts for ROP of the simpler *rac*- β -butyrolactone.^[8d] Although the definitive scenario of these electronic interactions could not be delineated yet, DFT computations performed on models of the active center suggest that halogen bonding between the β -alkoxybutyrate growing polyester chain and Cl(Br) moieties is probably not the driving force for the experimentally observed high syndioselectivity of the catalysts.

Experimental Section

General conditions

All manipulations were performed under inert atmosphere (argon, $< 3 \text{ ppm O}_2$) using standard Schlenk, vacuum line, and glovebox techniques. Solvents (toluene, tetrahydrofuran) were freshly distilled from Na/benzophenone under argon and degassed thoroughly by freeze-thaw-vacuum cycles prior to use. Bisphenol proligands and yttrium amide precursors **1a–d** were synthesized according to reported methods.^[8d] Isopropyl alcohol (Acros) was distilled over Mg turnings under argon atmosphere and kept over activated 3–4 Å molecular sieves. CDCl_3 was dried over a mixture of 3 and 4 Å molecular sieves. Racemic benzyl β -malolactonate (*rac*-MLA^{Bz}), benzyl (*S*)- β -malolactonate (*S*-MLA^{Bz}), racemic allyl β -malolactonate (*rac*-MLA^{All}), and racemic methyl β -malolactonate (*rac*-MLA^{Me}) were synthesized from aspartic acid according to reported procedures.^[15,27]

Instruments and measurements

^1H (500 and 400 MHz) and $^{13}\text{C}\{^1\text{H}\}$ (125 MHz) NMR spectra were recorded with Bruker Avance AM 500 and Ascend 400 spectrometers at 25°C . ^1H and $^{13}\text{C}\{^1\text{H}\}$ NMR spectra were referenced internally relative to SiMe_4 ($\delta = 0 \text{ ppm}$) using the residual solvent resonances.

Average molar mass ($M_{n,SEC}$) and dispersity ($D_M = M_w/M_n$) values of the PMLA^{Bz}s, PMLA^{All}s and PMLA^{Me}s were determined by size-exclusion chromatography (SEC) in THF at 30°C (flow rate = 1.0 mL min^{-1}) with a Polymer Laboratories PL50 apparatus equipped with a refractive index detector and a set of two Resi-Pore PLgel 3 μm MIXED-D $300 \times 7.5 \text{ mm}$ columns. The polymer samples were dissolved in THF (2 mg mL^{-1}). All elution curves were calibrated with 12 monodisperse polystyrene standards (M_n

range = 580–380,000 g mol⁻¹); $M_{n,SEC}$ values of the PMLA^{Bz}s, PMLA^{All}s, and PMLA^{Me}s were uncorrected for the possible difference in hydrodynamic radius versus polystyrene.

The molar mass values of PMLA^{Bz}s, PMLA^{All}s, and PMLA^{Me}s samples were also determined by ¹H NMR spectroscopic analysis in CDCl₃ from the relative intensities of the signals of the PMLA^{Bz} main-chain methine hydrogen signals (-OCH(CO₂Bz)CH₂, δ = 5.58 ppm), PMLA^{All} main-chain methine (-OCH(CO₂All)CH₂, δ = 5.52 ppm), PMLA^{Me} main-chain methine (-OCH(CO₂Me)CH₂, δ = 5.50 ppm), and those of the isopropyl chain-end (-OCH(CH₃)₂, δ = 1.24 ppm).

Monomer conversions were calculated from ¹H NMR spectra of the crude polymer samples in CDCl₃ by using the integration (*Int.*) ratio $Int_{PMLAR}/[Int_{PMLAR} + Int_{MLAR}]$ of the methine hydrogen signals (-OCH(CO₂R)CH₂: δ = 5.50–5.58 ppm for polymers and δ = 4.88 ppm for monomers).

MALDI-ToF mass spectra were recorded at the CESAMO (Bordeaux, France) with a Voyager mass spectrometer (Applied Biosystems) equipped with a pulsed N₂ laser source (337 nm) and a time-delayed extracted ion source. Spectra were recorded in the positive-ion mode using the reflectron mode and with an accelerating voltage of 20 kV. A THF solution (1 mL) of the matrix (*trans*-3-indoleacrylic acid, IAA; Aldrich, 99%) and a MeOH solution of the cationization agent (NaI, 10 mg mL⁻¹) were prepared. A fresh solution of the polymer samples in THF (10 mg mL⁻¹) was then prepared. The three solutions were then rapidly combined in a 1:1:10 v/v [matrix]/[sample]/[cationization agent] ratio. An aliquot (1–2 μ L) of the resulting solution was deposited onto the sample target and vacuum-dried.

Differential scanning calorimetry (DSC) analyses were performed with a Setaram DSC 131 apparatus calibrated with indium, at a rate of 10 °C min⁻¹, under continuous flow of helium (25 mL min⁻¹), using aluminum capsules. The thermograms were recorded according to the following cycles: -50 to 50 °C at 10 °C min⁻¹; 50 to -50 °C at 10 °C min⁻¹; -50 °C for 5 min; -50 to 200 or 250 °C at 10 °C min⁻¹; 200 to 30 °C at 10 °C min⁻¹.

Statistical analysis and model fitting were performed by using software OriginPro 8 from OriginLab Corporation and Mk1 and Mk2 models defined previously.^[18]

General procedure for the ROP of *rac*-MLA^R

In a typical experiment (Table 1, entry 3), a Schlenk flask was charged in a glovebox with a solution of complex **1a** (6.3 mg, 5.82 μ mol) in toluene (0.58 mL), then *i*PrOH (0.50 μ L, 5.82 μ mol, 1.0 equiv vs. **1a**) was added under stirring. After 5 min, *rac*-MLA^{Bz} was added rapidly (120 mg, 0.58 mmol, 100 equiv) and the mixture was stirred at 20 °C for the appropriate time. The reaction was quenched by addition of acetic acid (ca. 10 μ L of a 1.6 mol L⁻¹ solution in toluene). The resulting mixture was concentrated to dryness under vacuum and the conversion was determined by ¹H NMR spectroscopic analysis of the residue in CDCl₃. The crude polymer was then dissolved in CH₂Cl₂ (ca. 1 mL) and precipitated in cold pentane (ca. 5 mL), filtered and dried under vacuum at 45 °C overnight (typical isolated yield 90–95%). The final polymer was then analyzed by NMR, SEC, and DSC analyses (Table 1).

***i*PrO-PMLA^{Bz}-H**: ¹H NMR (500 MHz; CDCl₃, 25 °C): δ = 7.33 (br m, 5nH; C₆H₅), 5.55 (br m, 1nH; CH₂CH(CO₂Bz)O), 5.14 (br s, 2nH; OCH₂C₆H₅), 4.56 (br m, 1H; OCH(CH₃)₂), 2.94 (br m, 2nH; CHCH₂(O)O), 1.24 ppm (m, 6H; OCH(CH₃)₂) (Figure 5); ¹³C{¹H} NMR (125 MHz; CDCl₃, 25 °C): δ = 168.2–168.0 (C=O), 135.1 (C8), 128.3–128.7 (C9–11), 68.8 (C(O)CH₂CH(CO₂Bz)O), 67.6 (OCH₂C₆H₅), 65.7 ((CH₃)₂CHO), 35.4 (OC(O)CH₂CH), 20.9 ppm ((CH₃)₂CHO) (Figure S5).

***i*PrO-PMLA^{All}-H**: ¹H NMR (500 MHz; CDCl₃, 25 °C): δ = 5.88 (m, 1nH; CH₂CH=CH₂), 5.52 (m, 1nH; CH₂CH(CO₂All)O), 5.31 and 5.25 (d and d, J = 17 and 10 Hz, respectively (geminal proton-proton couplings were not observed), 2nH; CH₂CH=CH₂), 4.64 (d, J = 5 Hz, 2nH; CH₂CH=CH₂), 3.41 (m, 1H; (CH₃)CHO), 3.00 (m, 2nH; CH₂CH(CO₂All)O), 1.24 ppm (m, 6H; (CH₃)CHO) (Figure 6); ¹³C{¹H} NMR (125 MHz; CDCl₃, 25 °C): δ = 168.1 and 167.8 (C=O), 131.3 (CH₂CH=CH₂), 119.0 (CH₂CH=CH₂), 68.7 (CH₂CH(CO₂All)O), 66.4 (CH₂CH=CH₂), 41.8 ((CH₃)CHO), 35.4 (CH₂CH(CO₂All)O), 21.7 ppm ((CH₃)CHO) (Figure S6).

***i*PrO-PMLA^{Me}-H**: ¹H NMR (500 MHz; CDCl₃, 25 °C): δ = 5.50 (m, 1nH; CH₂CH(CO₂CH₃)O), 3.76 (m, 3nH; CH₂CH(CO₂CH₃)O), 3.45 (m, 1H; (CH₃)CHO), 3.01 (m, 2nH; CH₂CH(CO₂CH₃)O), 1.26 ppm (m, 6H; (CH₃)CHO) (Figure 2); ¹³C{¹H} NMR (125 MHz; CDCl₃, 25 °C): δ = 168.7 and 168.3 (C=O), 68.7 (CH₂CH(CO₂CH₃)O), 53.0 (CH₂CH(CO₂CH₃)O), 35.6 (CH₂CH(CO₂CH₃)O), 34.3 ((CH₃)CHO), 22.5 ppm ((CH₃)CHO) (Figure 3).

Computational details

All calculations were performed with the TURBOMOLE program package using density functional theory (DFT).^[28–31] The gradient corrected density functional BP86 in combination with the resolution identity approximation (RI)^[32,33] was applied for the geometry optimizations of stationary point. A triple- ζ zeta valence quality basis set def-TZVP was used for all atoms.^[34] The stationary points were characterized as energy minima (no negative Hessian eigenvalues) by vibrational frequency calculations at the same level of theory. The results of calculations (total electronic energies of eight intermediates and zero-point energy corrections) are presented in Figure 14 and Table S7.

Acknowledgements

The authors gratefully thank the CNRS and the Region Bretagne for supporting part of this research (Ph.D. grant to C.G.J.). We thank Romain Ligny for performing VT ¹H and DOSY NMR spectroscopic analysis of complex **1d**.

Keywords: density functional calculations · lactones · polymers · ring-opening polymerization · yttrium

- [1] J.-F. Lutz, M. Ouchi, D. R. Liu, M. Sawamoto, *Science* **2013**, *341*, 1238149.
- [2] J. W. Kramer, D. S. Treitler, E. W. Dunn, P. M. Castro, T. Roisnel, C. M. Thomas, G. W. Coates, *J. Am. Chem. Soc.* **2009**, *131*, 16042–16044.
- [3] C. G. Jaffredo, Y. Chapurina, S. M. Guillaume, J.-F. Carpentier, *Angew. Chem. Int. Ed.* **2014**, *53*, 2687–2691; *Angew. Chem.* **2014**, *126*, 2725–2729.
- [4] J.-F. Carpentier, *Angew. Chem. Int. Ed.* **2010**, *49*, 2662–2663; *Angew. Chem.* **2010**, *122*, 2720–2722.
- [5] S. M. Guillaume, E. Kirillov, Y. Sarazin, J.-F. Carpentier, *Chem. Eur. J.* **2015**, *21*, 7988–8003.
- [6] For leading reviews on stereoselective ROP of β -lactones, see: a) C. M. Thomas, *Chem. Soc. Rev.* **2010**, *39*, 165–173; b) J.-F. Carpentier, *Macromol. Rapid Commun.* **2010**, *31*, 1696–1705.
- [7] R. W. Lenz, Z. Jedlinski, *Macromol. Symp.* **1996**, *107*, 149–161.
- [8] a) C.-X. Cai, A. Amgoune, C. W. Lehmann, J.-F. Carpentier, *Chem. Commun.* **2004**, 330–331; b) A. Amgoune, C. M. Thomas, J.-F. Carpentier, *Macromol. Rapid Commun.* **2007**, *28*, 693–697; c) N. Ajellal, M. Bouyahyi, A. Amgoune, C. M. Thomas, A. Bondon, I. Pillin, Y. Grohens, J.-F. Carpentier, *Macromolecules* **2009**, *42*, 987–993; d) M. Bouyahyi, N. Ajellal, E. Kirillov, C. M. Thomas, J.-F. Carpentier, *Chem. Eur. J.* **2011**, *17*, 1872–1883; e) J. S. Klitzke, T. Roisnel, E. Kirillov, O. d. L. Casagrande, J.-F. Carpentier, *Organometallics* **2014**, *33*, 309–321; f) C. G. Jaffredo, M.

- Schmid, I. del Rosal, T. Mevel, P. W. Roesky, L. Maron, S. M. Guillaume, *Chem. Eur. J.* **2014**, *20*, 14387–14402.
- [9] P. T. Altenbuchner, A. Kronast, S. Kissling, S. I. Vagin, E. Herdtweck, A. Pçthig, P. Deglmann, R. Loos, B. Rieger, *Chem. Eur. J.* **2015**, *21*, 13609–13617.
- [10] For a recent review on [amino-alkoxy-bis(phenolate)] rare earth complexes and their use in ROP catalysis, see: J.-F. Carpentier, *Organometallics* **2015**, *34*, 4175–4189.
- [11] C. G. Jaffredo, S. M. Guillaume, *Polym. Chem.* **2014**, *5*, 4168–4194.
- [12] For this experiment, the monomer was purified by flash chromatography followed by three flash distillations. The fourth distillation always led to degradation of the monomer.
- [13] A. Amgoune, C. M. Thomas, S. Ilinca, T. Roisnel, J.-F. Carpentier, *Angew. Chem. Int. Ed.* **2006**, *45*, 2782–2784; *Angew. Chem.* **2006**, *118*, 2848–2850.
- [14] P. Guerin, M. Vert, C. Braud, R. Lenz, *Polym. Bull.* **1985**, *14*, 187–192.
- [15] P. Guerin, J. Francillette, C. Braud, M. Vert, *Makromol. Chem. Macromol. Symp.* **1986**, *6*, 305–314.
- [16] M. Helou, G. Moriceau, Z. W. Huang, S. Cammas-Marion, S. M. Guillaume, *Polym. Chem.* **2011**, *2*, 840–850.
- [17] C. G. Jaffredo, J.-F. Carpentier, S. M. Guillaume, *Macromolecules* **2013**, *46*, 6765–6776.
- [18] M. Sepulchre, *Makromol. Chem.* **1988**, *189*, 1117–1131. The Mk1 model expressions for triad sequences are: $(mm) = [m]^2$, $(rm) = (mr) = [mr]$ and $(rr) = [r]^2$. The probability of racemic linkage in the polymer chain is then defined by $P_r = \sqrt{(rr)}$.
- [19] Deconvolution performed using OriginPro 8 software from OriginLab Corporation.
- [20] $RMS = ((\sum(I_{obs} - I_{calcd})^2 / 8)^{0.5})$. The fidelity of the statistical model remained dependent of the regularity of the polymer analyzed.
- [21] a) P. Hormnirun, E. L. Marshall, V. C. Gibson, A. J. P. White, D. J. Williams, *J. Am. Chem. Soc.* **2004**, *126*, 2688–2689; b) P. Hormnirun, E. L. Marshall, V. C. Gibson, R. I. Pugh, A. J. P. White, *Proc. Natl. Acad. Sci. USA* **2006**, *103*, 15343–15348.
- [22] E. L. Marshall, V. C. Gibson, H. S. Rzepa, *J. Am. Chem. Soc.* **2005**, *127*, 6048–6051.
- [23] a) L. C. Gilday, S. W. Robinson, T. A. Barendt, M. J. Langton, B. R. Mullaney, P. D. Beer, *Chem. Rev.* **2015**, *115*, 7118–7195; b) G. Cavallo, P. Me-trangolo, R. Milani, T. Pilati, A. Priimagi, G. Resnati, G. Terraneo, *Chem. Rev.* **2016**, *116*, 2478–2601.
- [24] P. Auffinger, F. A. Hays, E. Westhof, P. S. Ho, *Proc. Natl. Acad. Sci. USA* **2004**, *101*, 16789–16794.
- [25] R. A. Gross, Y. Zhang, G. Konrad, R. W. Lenz, *Macromolecules* **1988**, *21*, 2657–2668.
- [26] C. E. Fernández, M. Mancera, E. Holler, J. A. Galbis, S. Muñoz-Guerra, *Polymer* **2006**, *47*, 6501–6508.
- [27] a) M.-A. Leboucher-Durand, V. Langlois, P. Guérin, *React. Funct. Polym.* **1996**, *31*, 57–65; b) S. Cammas, I. Renard, V. Langlois, P. Guérin, *Polymer* **1996**, *37*, 4215–4220.
- [28] R. Ahlrichs, M. Bär, M. Häser, H. Horn, C. Kölmel, *Chem. Phys. Lett.* **1989**, *162*, 165–169.
- [29] O. Treutler, R. Ahlrichs, *J. Chem. Phys.* **1995**, *102*, 346–354.
- [30] K. Eichkorn, O. Treutler, H. Öhm, M. Häser, R. Ahlrichs, *Chem. Phys. Lett.* **1995**, *242*, 652–660.
- [31] TURBOMOLE V6.2 2010, a development of University of Karlsruhe and Forschungszentrum Karlsruhe GmbH, 1989–2007, TURBOMOLE GmbH, since 2007; available from <http://www.turbomole.com>.
- [32] M. Sierka, A. Hogekamp, R. Ahlrichs, *J. Chem. Phys.* **2003**, *118*, 9136–9148.
- [33] P. Deglmann, K. May, F. Furche, R. Ahlrichs, *Chem. Phys. Lett.* **2004**, *384*, 103–107.
- [34] A. Schäfer, C. Huber, R. Ahlrichs, *J. Chem. Phys.* **1994**, *100*, 5829–5835.

Received: January 17, 2016

Published online on April 15, 2016